Analyst

PAPER

View Article Online
View Journal | View Issue

Cite this: *Analyst*, 2014, **139**, 5954

Enhanced live cell imaging *via* photonic crystal enhanced fluorescence microscopy†

Weili Chen,[a] Kenneth D. Long,[b] Hojeong Yu,[a] Yafang Tan,[a] Ji Sun Choi,[c] Brendan A. Harley[cd] and Brian T. Cunningham*[ab]

We demonstrate photonic crystal enhanced fluorescence (PCEF) microscopy as a surface-specific fluorescence imaging technique to study the adhesion of live cells by visualizing variations in cell–substrate gap distance. This approach utilizes a photonic crystal surface incorporated into a standard microscope slide as the substrate for cell adhesion, and a microscope integrated with a custom illumination source as the detection instrument. When illuminated with a monochromatic light source, angle-specific optical resonances supported by the photonic crystal enable efficient excitation of surface-confined and amplified electromagnetic fields when excited at an on-resonance condition, while no field enhancement occurs when the same photonic crystal is illuminated in an off-resonance state. By mapping the fluorescence enhancement factor for fluorophore-tagged cellular components between on- and off-resonance states and comparing the results to numerical calculations, the vertical distance of labelled cellular components from the photonic crystal substrate can be estimated, providing critical and quantitative information regarding the spatial distribution of the specific components of cells attaching to a surface. As an initial demonstration of the concept, 3T3 fibroblast cells were grown on fibronectin-coated photonic crystals with fluorophore-labelled plasma membrane or nucleus. We demonstrate that PCEF microscopy is capable of providing information about the spatial distribution of cell–surface interactions at the single-cell level that is not available from other existing forms of microscopy, and that the approach is amenable to large fields of view, without the need for coupling prisms, coupling fluids, or special microscope objectives.

Received 17th August 2014
Accepted 18th September 2014

DOI: 10.1039/c4an01508h

www.rsc.org/analyst

Introduction

The adhesive interaction of cells with extracellular matrix (ECM) is one of the most fundamental mechanisms through which cells communicate with their environment.[1] Cell–surface interactions play a critical role in a wide range of processes such as growth, migration, proliferation, apoptosis, and differentiation that occur during drug exposure, cell-to-cell communication,[2] the presence of chemical gradients,[3] introduction of growth factors, and programmed gene expression. Ultimately, these fundamental processes govern biological activity such as tissue growth, inflammation, wound healing and metastasis.[4,5] Changes in cell–ECM adhesion that result from changes in the local environment (such as *via* introduction of drugs, growth factors, or other cells) are a contributing factor in the progression of a variety of diseases.[6] While the significance of cell–substrate adhesion has been realized for years, there are few tools currently available that enable visualization and quantification of cell-to-surface coupling behavior.

Current approaches for imaging cell–substrate interactions primarily utilize fluorescent dyes that label specifically targeted cell structures, and fluorescent excitation methods that concentrate illumination energy within a confined zone that is in direct contact with adherent cells (see ESI, Table 1†). For example, total internal reflection fluorescence (TIRF) microscopy can selectively excite fluorophores near the adherent cell surface, while minimizing fluorescence originating from the bulk of the cell[7] through a spatially restricted evanescent field upon a substrate surface when total internal reflection occurs. While TIRF microscopy has been broadly adopted through the availability of specialized microscope objectives, the approach is not able to identify a locus of high fluorescence intensity that is bright because it is close to the cell–substrate interface or because it contains a high concentration of fluorescent dye.[8] Confocal microscopy is another important technique that is

[a]*Department of Electrical and Computer Engineering, University of Illinois at Urbana-Champaign, 208 North Wright Street, Urbana, IL, 61801, USA. E-mail: bcunning@illinois.edu*

[b]*Department of Bioengineering, University of Illinois at Urbana-Champaign, Urbana, IL, USA*

[c]*Department of Chemical and Biomolecular Engineering, University of Illinois at Urbana-Champaign, Urbana, IL, USA*

[d]*Institute for Genomic Biology, University of Illinois at Urbana-Champaign, Urbana, IL, USA*

† Electronic supplementary information (ESI) available. See DOI: 10.1039/c4an01508h

used to visualize features of cell membranes, in which a diffraction-limited focal volume of laser illumination is scanned through of the cell in three dimensions. Although confocal microscopy can specifically target volume elements of the cell that are close to the boundary with the surface, the approach also results in background excitation of components in the cell body that are above/below the focal plane. Further, the throughput of confocal microscopy for rapidly imaging many cells in a large field of view is limited by the necessity for scanning the focused spot.[9]

In order to address the limitations of TIRF and confocal microscopy, there has been intense interest in the development of surfaces and nanostructures that can more effectively couple light from a fluorescence excitation source, and spatially confine it to the region of a cell that adheres to the surface. These techniques can be advantageous because they can effectively amplify the excitation intensity beyond that available from an ordinary glass surface, resulting in greater fluorescent intensity than would be available from TIRF, given an identical illumination intensity.

While the first demonstrations of enhanced fluorescence appeared shortly after the discovery of surface enhanced Raman scattering almost three decades ago,[10–12] the application of this method to improving bioassays has only occurred recently, in conjunction with the increased use of fluorescence protocols in life science research. Enhancing fluorescence typically relies on an interaction between a fluorophore and a resonant optical structure, the most common of which are metal nanoparticles, smooth metal surfaces, and nanostructured metal surfaces that support plasmon resonances. These resonances can affect fluorophores in a variety of ways: they can amplify excitation light,[13] alter the spatial distribution of the fluorophore emission,[14] modify the radiative lifetime of the fluorophore,[15] or simultaneously perform more than one of these functions.[16–18] Metal nanostructures have been demonstrated to enhance fluorescence for applications such as immunoassays[19] and cell imaging.[20] However, fluorescence enhancement using metal surfaces or metal nanoparticles suffers from quenching if the fluorophore is too close to the metal, resulting in very stringent requirements for surface-fluorophore spacing.[21] The low quality-factor of metal-based resonances, due to optical absorption, further reduces the achievable amplification factor for metal-enhanced fluorescence.[22,23]

Photonic crystals (PCs), or periodic arrangements of materials with differing dielectric constants, represent a powerful class of substrates for enhancing fluorescence. The PCs used in our research are comprised of periodically modulated grating structure with low and high refractive index layers in which the period is smaller than the wavelength of light used to excite the structure (Fig. 1a). A resonance in this structure is excited when evanescent diffracted orders couple to modes of an effective high refractive index layer, and are re-radiated through diffraction in-phase with the reflected zeroth-order wave and out-of-phase with the transmitted zeroth-order wave.[24] The dispersion of the PC then reveals these resonances as sharp dips in the transmission spectrum (Fig. 1d) upon white light illumination, resulting from the coupling of light at specific incidence angles and wavelengths to the structure. These resonances are capable of enhancing fluorescence in a similar fashion to surface plasmon resonances, taking advantage of two phenomena: enhanced excitation and enhanced extraction. Enhanced excitation is the result of incident radiation coupling to a PC resonance, which increases the local electric field intensity throughout the structure. These fields decay exponentially as one moves away from the substrate surface (Fig. 1e and f), in a similar fashion to TIRF microscopy, but the resonance coupling provides a constructive interference effect that amplifies the incident wave.[25] Multiplied with this enhancement effect is enhanced extraction, whereby fluorophore emission is redirected along the PC dispersion[26] to increase the percentage of output photons that are available for detection. This mechanism helps to claim emitted light that otherwise may have been lost to guided modes within the substrate or to emission at oblique angles not collected by the detection optics. Overall, photonic crystal enhanced fluorescence (PCEF) provides an optically active surface capable of providing uniform fluorescence enhancement over large areas without the quenching effects that limit metal enhanced fluorescence approaches.

PCEF offers an additional unique feature that is not available in TIRF microscopy. For effective fluorescence enhancement by PCEF, the illumination angle of a monochromatic light source must be chosen to match with the resonant coupling angle of the PC.[27] However, by intentional adjustment of the incident angle to an off-resonant condition, one may obtain "ordinary" laser illumination, and thus it is easy to adjust the illumination between an "on-resonant" and an "off-resonant" state, effectively switching the enhancement effect on/off at will. In this work, we take advantage of this capability to create spatial maps of the PCEF enhancement factor of fluorescence-emitting regions on the surface and inside live cells. Rather than generating images of florescence intensity, as performed by TIRF, which results in fluorescence intensities that are dependent upon both the local dye concentration and the position of the emitters with respect to the substrate surface, PCEF microscopy creates fluorescence enhancement factor image, that derive their magnitude from the proximity of the fluorescent emitter from the surface (Fig. 1f). While previous publications have described the application of PCEF in the context of microarrays of biomolecular assays for multiplexed detection of soluble protein biomarkers,[28] gene expression,[29] and miRNA,[30] this work represents the first report of PCEF for fluorescence imaging of cells, in which alternating on/off-resonance images are used to derive maps of the surface engagement of cell structures at the single-cell level.

Methods

Fabrication method

The PC surfaces used in this study were prepared using a room-temperature nanoreplica molding fabrication approach, which has been used previously to produce PCs that are embedded into disposable labware such as microplates, microfluidic cartridges, and microscope slides.[31–34] Briefly, a molding

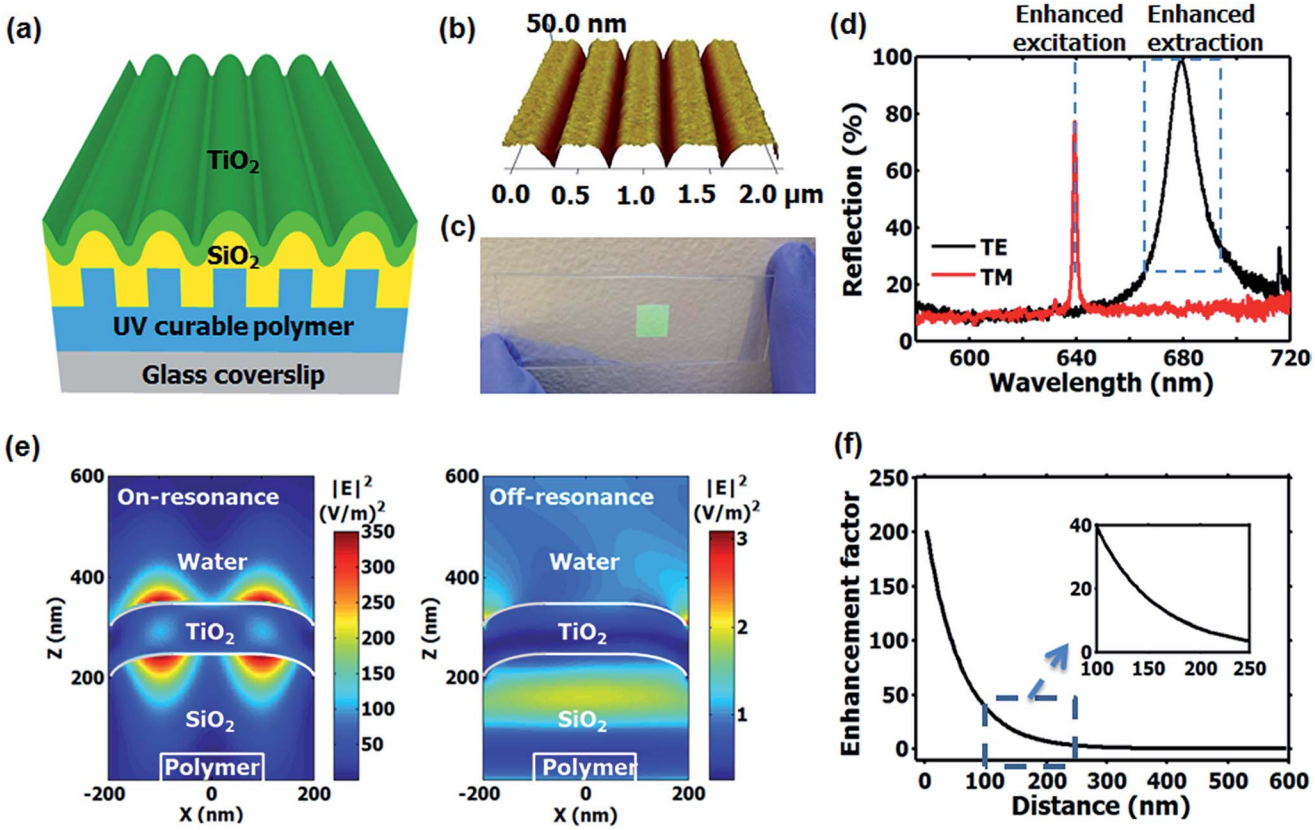

Fig. 1 (a) Schematic diagram of the PC; (b) AFM image of the PC surface showing a grating period of 400 nm and grating depth of 50 nm; (c) photograph of the PC, fabricated on a standard microscope slide. (d) Reflection spectrum of a PC. The red and black curves indicate the reflection response of the PC under illumination of TM or TE polarized light. (e) FDTD simulation of evanescent electric field distribution when the PC is under resonant (left) and non-resonant (right) illumination. The electrical field intensity under on-resonance condition is enhanced maximally 350 times compared to the incident light intensity, while the off-resonance electrical field exhibits little intensity increase. (f) The distance dependence of the enhancement factor.

template patterned with a negative volumetric image of the desired PC surface structure (Λ = 400 nm, d = 120 nm) is prepared with a silicon master wafer using deep ultraviolet lithography and reactive ion etching (RIE). This template can be used repeatedly to inexpensively produce uniform, single-use devices. To transfer the grating pattern from the master template to a PC, a small amount of liquid UV-curable polymer (UVCP) is squeezed between the template and a flexible glass coverslip (0.17 mm thick), followed by exposure to a high intensity ultraviolet lamp to solidify the polymer layer. The glass coverslip is initially treated with an adhesive coating (hexamethyldisilane (HMDS)), so the hardened polymer layer can preferentially adhere to glass coverslip when it is peeled away from the template. A RF sputtering system (PVD 75, Kurt Lesker) is used to apply the SiO_2 (~200 nm) and TiO_2 (~95 nm) layers. Finally, the glass coverslip with the PC is attached to a conventional glass microscope slide using adhesive (Norland 61).

Detection instrument

The detection instrument is configured to enable illumination of cells from beneath the PC, so cell bodies are not exposed to the illumination source when the PC is excited under the resonant coupling condition. The system is configured to provide a focused line of TM-polarized illumination that is only focused along the axis parallel to the grating lines, enabling all the light that enters the PC with an axis perpendicular to the grating lines to be incident at the same angle. This configuration is crucial for achieving efficient coupling of the laser to the PC, so all the incident light satisfies the on-resonant condition.[30,35] Using this approach, substantially large PC surface areas can be imaged by scanning the illumination line across the device.

Fig. 2 shows a schematic diagram of the detection system, which is built upon the body of a standard microscope (Carl Zeiss Axio Observer Z1). In addition to the light for ordinary bright field imaging, a second illumination path is provided from a semiconductor laser (λ = 637 nm, AlGaAs, 35 mW) to excite the fluorescent dye. The laser is coupled to a polarization maintaining (PM) fiber to provide a linearly-polarized beam, which is later collimated by a condenser lens yielding a laser beam with a diameter of 6.7 mm. A half-wave plate is then used to adjust the electric field polarization to be perpendicular to the PC grating lines, thus ensuring TM mode illumination. The output beam is focused by a cylindrical lens (f = 200 nm) to form a linear beam at the back focal plane of the objective lens

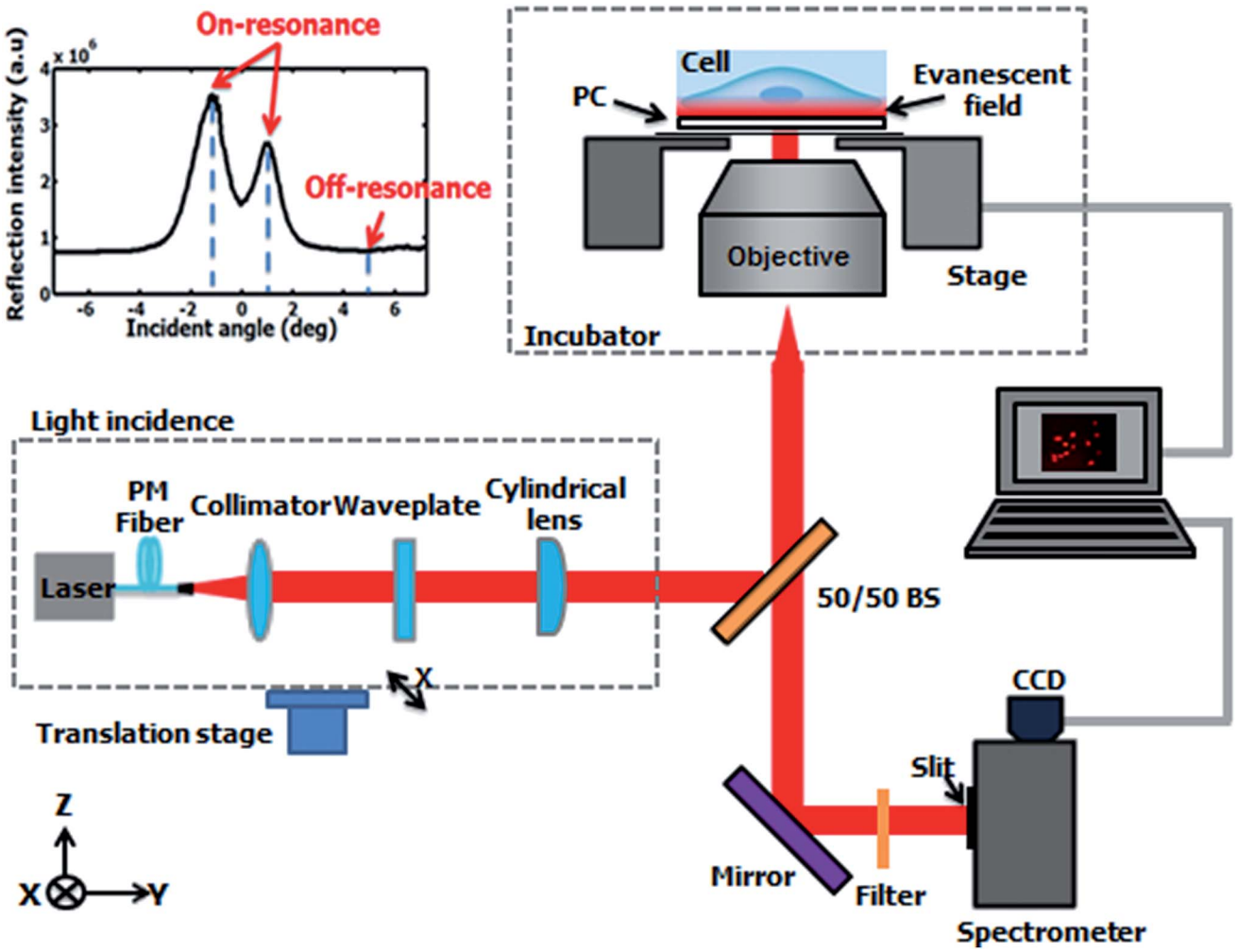

Fig. 2 Schematic diagram of the detection instrumentation. Illumination from a fiber coupled semiconductor laser diode is collimated and passed through a half waveplate to produce a polarization perpendicular to the PC grating lines. A cylindrical lens focusses the light to a line at the back focal plane of objective. The reflected light from PC is collected by a CCD camera after passing through an emission filter. The translation stage helps the adjustment of incident angle by moving the light source along the *x*-direction. (Top left) Angle reflection spectra of the PC when illuminated with a collimated semiconductor laser at 637 nm over a range of illumination angles. Maximum reflection intensity occurs at the on-resonance condition at an incident angle of ±1.14° from normal. The off-resonance condition refers to the laser illumination at an incidence angle of 5°.

(10×, Zeiss) *via* a 50/50 beamsplitter. After passing through the objective lens, the laser is focused along the direction parallel to the PC grating while remaining collimated in the direction perpendicular to the grating. The width of the illumination line is 6 μm, effectively minimizing the exposure of fluorophores in adjacent areas. The PC is placed on a motorized sample stage (MS2000, Applied Scientific Instruments) that moves in a direction perpendicular to the illumination line during experiments to cover a targeted area on the PC surface. The emitted fluorescence is collected by the objective (10×, Zeiss, focal length f = 16.45 mm) and projected, *via* a side port of the inverted microscope and a zoom lens onto an EM-CCD camera (Photometrics Cascade 512). An emission filter is placed in front of the camera to block the laser light coming from the source, which passes only the fluorescence emission photons. In order to match the resonance condition of the PC, an angle tuning capability is needed to adjust the incident angle of the laser light. For this purpose, an assembly including the end of the PM fiber, the collimator, the half waveplate and the cylindrical lens is mounted on a motorized translation stage (Zaber LSM-25) that shifts the incident light along the horizontal direction. The lateral position displacement (Δd) of the laser light focused at the back focal plane of the objective effectively leads to a change in the angle ($\Delta\theta$) of illumination for the PC surface given by $\Delta\theta = \tan^{-1}(\Delta d/f)$. The incident angle can be controlled from −10° to +10° with an increment of 0.03° by translating the motorized stage over a distance of 6 mm with a step size of 0.01 mm.

To construct a two-dimensional fluorescence image, the sample stage holding the PC translates along the axis perpendicular to the imaged line with an increment of 0.6 μm per step, while the camera gathers the fluorescence intensity of the center pixel line within the illuminated region at each step

position. Using this technique, a series of lines is assembled into an image at a rate of 0.1 s per line to form the whole image. After completing a scan, the stage can return to its starting position to repeat the scan using a second incident angle. The pixel resolution along the scan direction is determined by the step increment (0.6 μm) and the pixel resolution in the other direction is also 0.6 μm, as determined by the camera resolution and effective optical magnification of the system. Each image is comprised of 512 × 512 pixels covering a 307 × 307 μm region on the PC surface.

Cell culture and fluorophore loading

The 3T3 fibroblasts (ATCC) were cultured in DMEM media with 5% fetal bovine serum. Silicone rubber gaskets (prepared using polydimethylsiloxane (PDMS)) were attached to the sensor surface to provide a media containment (1 mL volume). Prepared slides were treated with oxygen plasma, and incubated with 10 μg mL^{-1} fibronectin to encourage attachment. Cells were incubated on the PC surface for 12 hours prior to labelling with fluorescent dyes. For membrane staining, a non-lectin, amphipathic membrane dye that fluoresces at a wavelength of λ = 666 nm (Life Technologies, excitation/emission: 659/674 nm) was added at 1× concentration to the chamber and incubated for 10 minutes. Afterward, the chamber was rinsed with DMEM culture media. For nuclear staining, a cell-permanent nuclear stain that binds to DNA and fluoresces at λ = 647 nm (Life Technologies, excitation/emission 638/686 nm) was added to the chamber, and incubated for 30 minutes before imaging. Imaging was completed on the instrument as described above with the microscope stage enclosed within an environmentally-controlled incubation chamber (Zeiss) maintaining constant 37°C temperature and 5% CO_2.

Results

PC biosensor design and structure

A schematic diagram the PC structure is shown in Fig. 1a. The PC is comprised of a subwavelength grating structure formed in an ultraviolet curable polymer (UVCP) layer of low refractive index on a glass coverslip substrate. The polymer grating structure is coated with a ~200 nm silicon dioxide (SiO_2) spacer layer followed by a ~95 nm titanium dioxide (TiO_2) thin film with high refractive index (n = 2.35), acting as the optical confinement layer to support establishment of a narrow bandwidth single-mode resonant reflection at a wavelength of λ = 635 nm when the device is covered in aqueous media, and illuminated at normal incidence. At specific combinations of incident wavelength and angle of incidence, the PC surface will reflect nearly 100% of the incident light, as an electromagnetic standing wave is generated that extends from the PC surface and into the surrounding media. Surface-confined electromagnetic fields at the resonant coupling condition are intensified, compared to the field intensity of the illumination source, resulting in surface-localized fluorophores experiencing greater excitation than would be achieved without the presence of the nanostructure, or for "off-resonance" illumination that does not match the resonant coupling condition of the PC. In this work, the PC was intentionally designed to interact efficiently with a laser in the red part of the optical spectrum (λ = 637 nm), which coincides with the excitation wavelength of fluorophores for labelling cell structures. The approach described here may be extended to any other wavelength from UV[36] to IR[37] by selection of the PC period, and we have demonstrated that a single PC may be used to excite fluorophores with multiple excitation wavelengths.[38] The PCs used for all experiments reported here have a grating period of Λ = 400 nm, depth of d = 50 nm, and duty cycle of f = 50%. The dimensional parameters were verified by atomic force microscopy (Fig. 1b). The PC was fabricated as a 9 × 9 mm^2 region on the surface of a conventional glass microscope slide, as shown in Fig. 1c.

In this study, the PC surface is engineered to exhibit strong optical resonance at both the excitation (λ_{ex} = 637 nm) and emission (λ_{em} ~ 680 nm) wavelengths for dyes in the general spectral range of cyanine-5 (Cy5) by utilizing two orthogonal polarization modes of light: transverse magnetic (TM) and transverse electric (TE). The electric field component of the TM mode is perpendicular to the grating lines in the PC, while that of the TE mode is parallel to the grating lines. Fig. 1d shows the reflection spectrum of a PC under white light illumination at normal incidence, in which each reflection peak indicates a resonance. Compared to the TE resonance with half-width of $\Delta\lambda$ = 14.3 nm, the TM resonance has a much narrower linewidth ($\Delta\lambda$ = 1.5 nm), implying a higher resonance quality factor, which is related to the ratio between the energy stored in a resonance and the energy dissipated. Thus, we design the TM mode to provide the enhanced excitation effect. The TE resonance, on the other hand, is designed to overlap with the fluorescence emission spectrum with a resonant angle of 0° (relative to surface normal) as the collection optics is oriented perpendicular to the sample surface. The fluorescence output efficiently coupled to the TE mode is channeled preferentially away from the PC at an angle normal to the surface, significantly improving the collection efficiency for fluorescent emission photons that originate from the PC surface. While the enhanced excitation effect can be turned off by illuminating the PC at an off-resonant angle, the enhanced extraction effect is always active for emitters on the PC surface that match the TE mode wavelength.

FDTD simulation

To characterize the resonant response of the PC under illumination from a TM polarized laser, a commercially available electromagnetic simulation package (FDTD Solutions, Lumerical Inc.) was used to study the optical field distribution (normalized to incident intensity) and the distance dependence of the enhancement effect. Since the fluorophores interact with excitation light primarily through excitation of their internal electrons, only electric field components are considered. One period of the PC structure was studied with a periodic boundary condition applied along the direction perpendicular to the grating lines, as shown in Fig. 1e.

To simulate the electric field associated with the PC used in experiments, the corners of grating were slightly rounded to match the shape observed *via* AFM, and the superstrate material was chosen to represent water ($n_{water} = 1.33$). The illumination is provided by a monochromatic plane wave light source at a wavelength $\lambda = 637$ nm, (the same wavelength used for experiments) and a magnitude, represented by the power of the incident electric field of $|E|^2 = 1\ (\mathrm{V\ m^{-1}})^2$. In our simulation, the on-resonance incident angle for a wavelength of $\lambda = 637$ nm is designed to be 0° (normal incidence). Fig. 1e (left) shows the spatial distribution of the near-field electric field at the resonance condition. The resonant electromagnetic standing wave generates surface-confined electric field power with magnitudes as high as $|E|^2 = 100$–$300\ (\mathrm{V\ m^{-1}})^2$ in proximity to the TiO_2 layer with the evanescent tails penetrating both the substrate and superstrate materials. To demonstrate the difference between the on-resonance and the off-resonance condition, a second simulation was performed for the identical device structure and illumination source, but incident at an off-resonant coupling angle 5° from normal. As shown in Fig. 1e (right), the enhancement effect is generally eliminated due to the mismatch of incidence angle with the resonant coupling angle and the near-field electric field intensity is very close to $|E|^2 = 1\ (\mathrm{V\ m^{-1}})^2$. The distance dependence of the enhancement factor was estimated through simulation. The enhancement factor at a particular height was calculated as the ratio between the averaged electric field intensity at on- and off-resonance conditions, and is plotted as a function of the distance above the PC surface ranging from 2 nm to 600 nm, as shown in Fig. 1f. As expected, the enhancement effect decays exponentially as the fluorescent emitter is translated vertically from the PC surface, with the enhancement effect nearly completely eliminated for distances from the surface greater than 500 nm. Importantly, the enhancement factor at each vertical distance is unique, suggesting that we can estimate the distance between a fluorescent emitter and the PC surface by measuring the fluorescence intensity at both on- and off-resonance and calculating the enhancement factor.

Fluorescent enhancement-factor cell imaging

In order to characterize the adhesion properties of live cells and demonstrate the enhanced fluorescence imaging capability of PCEF microscopy, 3T3 fibroblast cells were cultured and observed when they are adherent to fibronectin-treated PC surfaces. Fibroblasts are the most common resident cells in connective tissue. Upon injury, fibroblast cells near the wound proliferate and produce large amounts of collagenous matrix to help isolate and repair the damaged tissue.[39] The cell line was selected for initial demonstration of PCEF microscopy due to its broad utility in tissue engineering and clinical applications. Cellular functions such as cell migration, division, endocytosis and exocytosis usually involve changes in the arrangement and interaction of specific molecules and organelles. These changes occur not only in the plane of the cell–substrate interface but also in the dimension perpendicular to the substrate. Therefore, it is important to analyze the activities and distribution in three dimensions of specific molecules and organelles in living cells during normal functions.

When illuminated with the $\lambda = 637$ nm laser, the excitation efficiency for the nuclear dye is nearly 100%, but for the membrane dye, the excitation efficiency is expected to be ~50%. Before each scan, an angle reflection spectrum is obtained, as shown in Fig. 2 (top left), to determine the incident angle of optimal on-resonant coupling from the laser. The averaged intensity of the laser light reflection from the PC surface is plotted as a function of the incident angle, and the peak in the angle reflection spectrum is an indicator of the occurrence of optical resonant coupling of the incident light to the PC, which also leads to a heightened energy density on the PC surface. The experimentally measured on-resonance incident angle is ±1.14 degrees. The two peaks observed in the spectrum are the result of bilateral symmetry of the PC along the grating lines, which means that the incident angle can be equivalently coupled into the resonance mode from two symmetrical angles. The off-resonance incident angle is selected to be 5 degrees away from the angle for resonant light coupling.

In order to avoid overestimation of the enhancement factor due to the effects of photobleaching (which will result in lower intensity images obtained with the second scan), the off-resonance scan is always performed first, followed by the on-resonance scan of the same field of view. Other than the angle of incidence, all other instrument settings were identical between the two scans. To quantify the fluorescence intensity loss after the first off-resonance scan, a photobleaching test was performed by scanning the fluorophore-labelled cells across the same field of view multiple times at a fixed off-resonance incident angle (see ESI, Fig. 1†). For the plasma membrane dye, the averaged fluorescence intensity measured from the second off-resonance scan is 64% of the first scan; while for the nuclear dye, nearly 93% of the fluorescence intensity is maintained in the second scan. Therefore, the fluorescence enhancement effect is underreported by a known factor that can be accounted for in our analytical model of the distance of the fluorophore from the PC surface.

(i) Modelling fluorescence enhancement in the cell contact region. To investigate the relationship between the fluorescence enhancement effect and the vertical location of a fluorophore-labelled cell component, a quantitative analysis of the absolute separation distance between the cell membrane/nucleus and the substrate is applied using a mathematical model that describes the evanescent electric field generated by the PC resonance. Consider an anchorage-dependent cell adhering to the aqueous side of the PC/cell media interface that is sequentially illuminated by off- and on-resonance incident light. The enhancement of the fluorescence intensity can be assumed to be only caused by the amplification of the electric field experienced by the fluorophores since the concentration of the fluorescent dye is the same between the two illuminations. The electric fields excited by the on-resonant illumination and the 5° off-resonant illumination for the PC device have been characterized by the FDTD simulation (Fig. 1e) that deduces an exponentially decaying curve for the relationship between the electric field enhancement factor and the vertical distance

above the PC surface. The curve can be fit by a simple exponential function:

$$\mathrm{EF} = \mathrm{EF}_0 \exp\left(-\frac{z}{d}\right), \quad (1)$$

where EF is the enhancement factor of the electric field intensity, EF_0 is the initial enhancement constant, z is the vertical distance relative to the PC surface and d is the penetration depth of the evanescent field. In this work, the cell membrane dye is used to label the plasma membrane at the cell boundaries, which is a very thin layer relative to the wavelength of the laser (*e.g.* 4 nm/637 nm = 0.006), so the electric field intensity is approximately constant throughout the membrane[40] and the averaged vertical location of the labelled membrane z_{mem} can be directly derived from (1) as:

$$z_{\mathrm{mem}} = d \ln\frac{\mathrm{EF}_0}{\mathrm{EF}}, \quad (2)$$

where the EF measured in the experiment is underestimated by a factor of α due to the photobleaching effect. On the other hand, the fluorescence enhancement effect for cell nucleus dye used in this work is determined by the overlap integral of the decaying evanescent intensity and the volume of distribution of the fluorophores of dye-labelled DNA within the nucleus.[41] Since the evanescent field can penetrate only the bottom portion of the cell and the nucleus is located nominally in the center of the cell, the enhancement factor for the cell nucleus dye can be calculated as an integral from the lower bound of the cell nucleus z_{nuc} to infinity to simplify the numerical analysis:

$$\mathrm{EF} = \int_{z_{\mathrm{nuc}}}^{\infty} \mathrm{EF}_0 \exp\left(-\frac{z}{d}\right)\mathrm{d}z = \mathrm{EF}_0 d \exp\left(-\frac{z_{\mathrm{nuc}}}{d}\right), \quad (3)$$

and

$$z_{\mathrm{nuc}} = d \ln\frac{\mathrm{EF}_0 d}{\mathrm{EF}}. \quad (4)$$

The two different equations describing the relationship between the fluorescence enhancement factor and the vertical location of the fluorescence emitters for the plasma membrane dye and the nucleus dye thus are determined by the different spatial distribution of fluorescent emitters. This model can be applied to estimate the separation distance between the labelled cell component and the substrate PC surface as shown by the following two imaging experiments.

(ii) Fluorescence imaging of cell membrane. Fig. 3a is a bright field image of 3T3 fibroblasts incubated on a PC surface showing a stretched cellular morphology featuring membrane protrusions (lamellipodia) consistent with substrate attachment. The cells also exhibit mostly round or ovalular nucleus contour. The off-resonance fluorescence image of the labelled cell membranes was taken first (Fig. 3b), showing clear cellular attachment patterns, with a high degree of similarity to the brightfield image. The high intensity regions in the image indicate the locations with a high concentration of plasma membrane dye since the excitation electric field under off-resonance state has little correlation to the vertical distance from the PC surface. Immediately after the off-resonance scan, the incident angle of the excitation laser was tuned to the

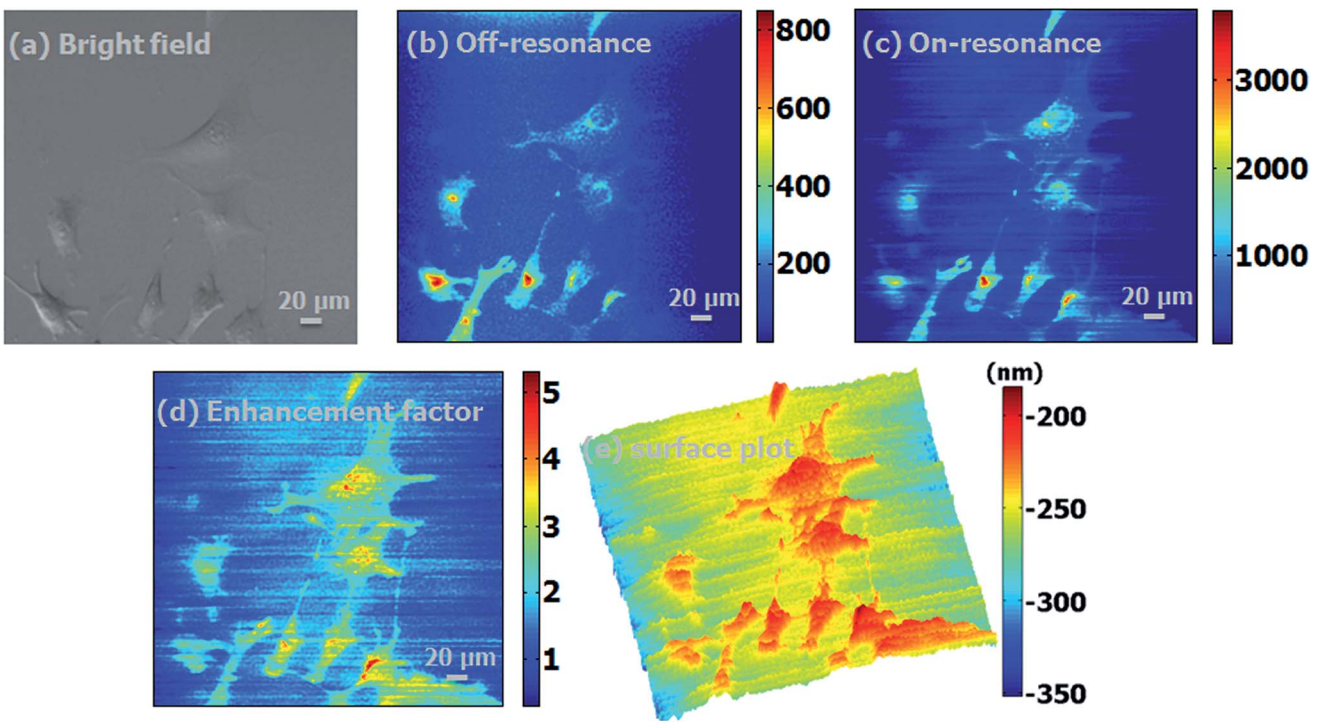

Fig. 3 Images of membrane-dye stained 3T3 fibroblast cells: (a) bright field, (b) off-resonance, (c) on-resonance, (d) enhancement factor image, (e) 3D surface plot image of the enhancement factor.

resonant angle of the PC for an on-resonance scan of the same field of view, as shown in Fig. 3c, where the output fluorescence intensity is related to the combined effects of the distance-dependent electric field and the local dye concentration. By comparing the two images, fluorescence intensity enhancement is achieved *via* the resonant illumination of the PC surface. To quantify the intensity amplification effect at each pixel position, an enhancement factor image was generated by dividing the on-resonance net intensity by the off-resonance net intensity (Fig. 3d), with an up to 5-fold enhancement in fluorescent signal achieved *via* this method.

Important information about cell adhesion can be inferred from the enhancement factor image. The data contained in the enhancement factor image, other than providing the spatial profiles of cell adhesion, can also be used to evaluate the strength of the formed cellular binding to the PC surface. The non-uniformity of the fluorescence signal shown for the plasma membrane dye is a result of the variance in vertical distance from the PC surface, and can be modeled with an understanding of the exponential decay of enhancement in the evanescent region of the PC. The enhancement factor image of the examined cells shows several regions of intense enhancement in the middle of the cells that do not correspond one-to-one with the high intensity regions in either the off-resonance or on-resonance fluorescence image. Many of the contact regions of the cell body, especially the ones near the cell nucleus, show average fluorescence intensity in the fluorescence images but experience the highest enhancement in the enhancement factor image. This result suggests that the plasma membrane within these areas is located closest to the PC surface, which could be a result of the cytoskeletal stress from the nucleus above it.[42] The contact regions of the lamellipodia, which are very thin and contain a low concentration of plasma membrane dye, are relatively low intensity regions in both the fluorescence image and fluorescence enhancement image. This would agree with a previous finding that lamellipodia are weakly adherent, with the strongest adhesion occurring at the periphery of lamellipodia.[43] Such results can be observed more clearly when the enhancement factor plot is presented in three dimensions (Fig. 3e) to resolve the spatial contours of the cell membrane that contacts the PC surface as calculated by eqn (2) with the parameters $EF_0 = 201$, $d = 58$ nm and $\alpha = 0.64$.

(iii) Fluorescence imaging of cell nucleus. To explore the effects that would be measured by a PCEF image when internal components of cells are labelled, we performed a second experiment using fluorescently stained nuclei. The bright field, on-resonance, off-resonance and enhancement factor images are shown in Fig. 4a–e. The cellular morphology exhibited in the brightfield image (Fig. 4a) corresponds well with that of previously studied stationary cells as the cell bodies are centrally located and surrounded by well-spread lamellipodia.[44] Cell spreading was not as extensive as observed when using the plasma membrane dye. In contrast to the expected irregular morphological fluorescence patterns stemming from cell membrane shapes, the labelled nuclei appear to be circular in the off- and on-resonance fluorescence images, as expected. The fluorescence intensity under off-resonance illumination (shown in Fig. 4b) is very low due to the weak excitation energy and the

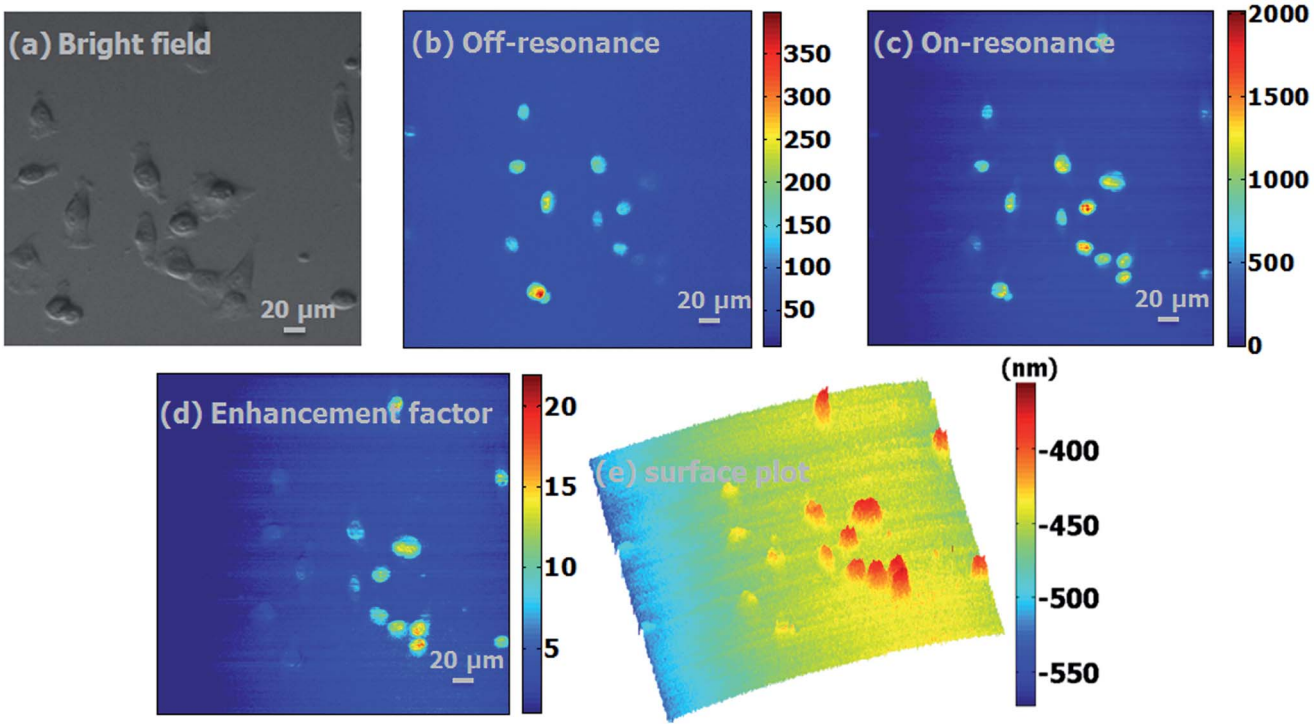

Fig. 4 Images of nuclear-dye stained 3T3 fibroblast cells: (a) bright field, (b) off-resonance, (c) on-resonance, (d) enhancement factor image, (j) 3D surface plot image of the enhancement factor.

spacing between the nucleus and the cell-substrate interface. However, when the incident angle is on-resonance (Fig. 4c), the penetration of the evanescent field into the cytoplasm is greatly increased and the emission of the fluorophores in the bottom portions of cell nuclei located within the evanescent field is enhanced up to 20 times the intensity observed in the off-resonance fluorescence image (Fig. 4d). According to eqn (4), the spatial distribution of the bottom surface of the labelled nuclei is plotted in Fig. 4e based on the fluorescence enhancement factor image with the parameters $EF_0 = 201$, $d = 58$ nm, and $\alpha = 0.92$. As observed in PCEF images of stained cell membranes, the high intensity regions in the single scan fluorescence images are not always spatially consistent with the high intensity regions in the enhancement factor image. The estimation of vertical distance between emitter and the PC surface based on the enhancement factor can efficiently remove the influence brought by the nuclear dye concentration. For example, the cell in the bottom-left has an illuminated region with above average brightness in both the off- and on-resonance image, indicating a relatively high concentration of fluorescent dye at that position, but has a below average value in the enhancement factor image, suggesting increased distance between PC surface and nuclei compared to other cells. Additionally, we observe that the enhancement effect within a single cell is not uniform, with the strongest enhancement occurring near the center of the nucleus and gradually weakening towards the periphery.

Conclusion

This work demonstrates a sensor structure, imaging detection instrument, and image processing approach termed "PCEF microscopy" that provides a new tool for imaging and quantifying the interaction between fluorescently-labelled cell components and surfaces that cells are attached to. PCEF microscopy provides quantitative information about the vertical location of specific cellular components relative to the cell adhesion surface, as the resonantly excitation electric field supported by the PC has a strong dependence on the spatial location and can be switched between on/off-resonance states by changing the angle of monochromatic illumination. The pixel intensity in the enhancement factor image is determined by the gap between the labelled cellular component and the PC substrate and it is not related to the local concentration of fluorescent dye. To interpret the enhancement factor image, a numerical analysis of the spatial distribution of the fluorophores and the corresponding fluorescence enhancement effect is applied, which allows for the visualization of the profiles of cell nucleus surface and the cell plasma membrane surface in three dimensions in the context of cell adhesion. The separation distance between cell membrane and its substrate for the cell-ECM contact sites has been reported to be larger than 100 nm.[45] In our experiments, the major parts of the cell membrane are approximately 100–300 nm from the PC substrate and most of the cell nuclei are about 300–500 nm above the PC substrate.

The cell–substrate separation distance is an important parameter in the characterization of cellular morphology and the efficiency of cell adhesion to an extracellular matrix. Adhesion strength is highly non-uniform within an individual cell, and it changes dynamically as a function of time, as cells undergo processes of their life cycle. The observation of cell adhesion through PCEF microscopy can provide rich information about the spatial locations of cellular components that are not available with other forms of microscopy, allowing for the investigation of cell–substrate interactions in several biologically relevant applications. For example, the capability described in this work may be used to study the role of the surface functionalization on cell attachment. By coating the sensor surface with different ECM molecules, the differences in cell attachment behavior may be directly observed. By completing time-course studies of cell attachment, information about how chemical or mechanical changes in the media/substrate environment affect cellular motion and behavior can be studied.

Except for the measurements of cell–substrate topology, PCEF microscopy can also be used to quantitatively estimate the location of the fluorescently labelled cell organelles or molecules inside the cell body that are located within the evanescent field above the PC surface. The evanescent field induced by the on-resonance excitation penetrates into the cell body adjacent to the cell–substrate interface, and is capable of exciting fluorophores residing in the immediate region near the interface. Specific cellular components associated with cell adhesion such as nucleus, cytoskeleton and membrane proteins can be selectively labelled or stained and then examined by PCEF microscopy to identify the vertical position of these targets of interest within the cell, which helps provide a better understanding about the spatial organization of cellular structures during the period of cell adhesion.

Cell adhesion to the substrate is implicated in differences in cellular shape, size and sub-cellular organization of organelles, which serves as a valuable indicator of viability as well as a sensitive indicator of cellular response to the external environment.[46] To track the location of specific cellular components or proteins involved in the cellular attachment process is challenging, especially in the context of complex and dynamic cell–ECM interactions such as neutrophil polarization and chemotaxis. PCEF microscopy provides a novel methodology for the investigation of those attributes in these cellular processes without the need for coupling prisms, spatial pinhole, or special microscope objectives. Due to the wide spectral tunability of the resonant wavelength of the PC structure, this microscopy approach can be extended to work with most of the fluorescent dyes used in cell biology.

Acknowledgements

The authors gratefully acknowledge funding from National Science Foundation (NSF CBET 11-32301) and the NCI Alliance for Nanotechnology in Cancer Midwest Cancer Nanotechnology Training Center (NIH Grant R25 CA154015A) for this work. Any opinions, findings, and conclusions or recommendations in

this work are those of the authors and do not necessarily reflect the views of the National Science Foundation.

References

1 M. Gardel and U. Schwarz, *J. Phys.: Condens. Matter*, 2010, **22**, 190301.
2 G. Pattabiraman, E. A. Lidstone, K. Palasiewicz, B. T. Cunningham and D. S. Ucker, *Mol. Biol. Cell*, 2014, **25**, 1704–1714.
3 M. Zelzer, R. Majani, J. W. Bradley, F. R. A. J. Rose, M. C. Davies and M. R. Alexander, *Biomaterials*, 2008, **29**, 172–184.
4 M. Barczyk, S. Carracedo and D. Gullberg, *Cell Tissue Res.*, 2010, **339**, 269–280.
5 N. J. Boudreau and P. L. Jones, *Biochem. J.*, 1999, **339**, 481–488.
6 U. Cavallaro and G. Christofori, *Biochim. Biophys. Acta, Rev. Cancer*, 2001, **1552**, 39–45.
7 D. Axelrod, *Traffic*, 2001, **2**, 764–774.
8 F. Lanni, A. S. Waggoner and D. L. Taylor, *J. Cell Biol.*, 1985, **100**, 1091–1102.
9 B. Joshi, S. S. Strugnell, J. G. Goetz, L. D. Kojic, M. E. Cox, O. L. Griffith, S. K. Chan, S. J. Jones, S. P. Leung, H. Masoudi, S. Leung, S. M. Wiseman and I. R. Nabi, *Cancer Res.*, 2008, **68**, 8210–8220.
10 W. H. Weber and C. F. Eagen, *Opt. Lett.*, 1979, **4**, 236–238.
11 A. M. Glass, P. F. Liao, J. G. Bergman and D. H. Olson, *Opt. Lett.*, 1980, **5**, 368–370.
12 W. Knoll, M. R. Philpott, J. D. Swalen and A. Girlando, *J. Chem. Phys.*, 1981, **75**, 4795–4799.
13 Y.-J. Hung, I. I. Smolyaninov and C. C. Davis, *Opt. Express*, 2006, **14**, 10825–10830.
14 I. Gryczynski, J. Malicka, Z. Gryczynski and J. R. Lakowicz, *Anal. Biochem.*, 2004, **324**, 170–182.
15 O. L. Muskens, V. Giannini, J. A. Sanchez-Gil and J. G. Rivas, *Nano Lett.*, 2007, **7**, 2871–2875.
16 J. R. Lakowicz, *Anal. Biochem.*, 2001, **298**, 1–24.
17 Y. Liu and S. Blair, *Opt. Lett.*, 2003, **28**, 507–509.
18 Y. Chen, K. Munechika and D. S. Ginger, *Nano Lett.*, 2007, **7**, 690–696.
19 J. Zhang, E. Matveeva, I. Gryczynski, Z. Leonenko and J. R. Lakowicz, *J. Phys. Chem. B*, 2005, **109**, 7969–7975.
20 J. Zhang, Y. Fu, D. Liang, R. Y. Zhao and J. R. Lakowicz, *Langmuir*, 2008, **24**, 12542–12457.
21 J. Zhang, Y. Fu, M. H. Chowdhury and J. R. Lakowicz, *Nano Lett.*, 2007, **7**, 2101–2107.
22 T. Hayakawa, S. T. Selvan and M. Nogami, *Appl. Phys. Lett.*, 1999, **74**, 1513–1515.
23 S. T. Selvan, T. Hayakawa and M. Nogami, *J. Phys. Chem. B*, 1999, **103**, 7064–7067.
24 D. Rosenblatt, A. Sharon and A. A. Friesem, *IEEE J. Quantum Electron.*, 1997, **33**, 2038–2059.
25 N. Ganesh, P. C. Mathias, W. Zhang and B. T. Cunningham, *J. Appl. Phys.*, 2008, **103**, 083104.
26 N. Ganesh, I. D. Block, P. C. Mathias, W. Zhang, E. Chow, V. Malyarchuk and B. T. Cunningham, *Opt. Express*, 2008, **16**, 21626–21640.
27 V. Chaudhery, M. Lu, A. Pokhriyal, S. C. Schulz and B. T. Cunningham, *IEEE Sens. J.*, 2012, **12**, 1272–1279.
28 C. S. Huang, S. George, M. Lu, V. Chaudhery, R. M. Tan, R. C. Zangar and B. T. Cunningham, *Anal. Chem.*, 2011, **83**, 1425–1430.
29 P. C. Mathias, S. I. Jones, H. Y. Wu, F. Yang, N. Ganesh, D. O. Gonzalez, G. Bollero, L. O. Vodkin and B. T. Cunningham, *Anal. Chem.*, 2010, **82**, 6854–6861.
30 S. George, V. Chaudhery, M. Lu, M. Takagi, N. Amro, A. Pokhriyal, Y. F. Tan, P. Ferreira and B. T. Cunningham, *Lab Chip*, 2013, **13**, 4053–4064.
31 C. J. Choi and B. T. Cunningham, *Lab Chip*, 2007, **7**, 550–556.
32 M. Lu, S. J. Park, B. T. Cunningham and J. G. Eden, *J. Microelectromech. Syst.*, 2007, **16**, 1397–1402.
33 C. J. Choi, I. D. Block, B. Bole, D. Dralle and B. T. Cunningham, *IEEE Sens. J.*, 2009, **9**, 1697–1704.
34 W. L. Chen, K. D. Long, M. Lu, V. Chaudhery, H. Yu, J. S. Choi, J. Polans, Y. Zhuo, B. A. C. Harley and B. T. Cunningham, *Analyst*, 2013, **138**, 5886–5894.
35 V. Chaudhery, M. Lu, C. S. Huang, J. Polans, R. M. Tan, R. C. Zangar and B. T. Cunningham, *Opt. Lett.*, 2012, **37**, 2565–2567.
36 N. Ganesh, I. D. Block and B. T. Cunningham, *Appl. Phys. Lett.*, 2006, **89**, 023901.
37 J. N. Liu, M. V. Schulmerich, R. Bhargava and B. T. Cunningham, *Opt. Express*, 2011, **19**, 24182–24197.
38 A. Pokhriyal, M. Lu, C. S. Huang, S. Schulz and B. T. Cunningham, *Appl. Phys. Lett.*, 2010, **97**, 121108.
39 B. Alberts, A. Johnson, J. Lewis, M. Raff, K. Roberts and P. Walter, *Molecular biology of the cell*, Garland Science, New York, 4th edn, 2002, 1467–1468.
40 W. Reichert and G. Truskey, *J. Cell Sci.*, 1990, **96**, 219–230.
41 J. S. Burmeister, L. A. Olivier, W. Reichert and G. A. Truskey, *Biomaterials*, 1998, **19**, 307–325.
42 K. N. Dahl, A. J. S. Ribeiro and J. Lammerding, *Circ. Res.*, 2008, **102**, 1307–1318.
43 E. S. Chhabra and H. N. Higgs, *Nat. Cell Biol.*, 2007, **9**, 1110–1121.
44 R. Badley, J. Couchman and D. Rees, *J. Muscle Res. Cell Motil.*, 1980, **1**, 5–14.
45 W.-T. Chen and S. Singer, *J. Cell Biol.*, 1982, **95**, 205–222.
46 B. Geiger, J. P. Spatz and A. D. Bershadsky, *Nat. Rev. Mol. Cell Biol.*, 2009, **10**, 21–33.